PROCEEDINGS OF SCIENCE

Reactor Neutrino Experiments

Achim Stahl*RWTH Aachen University

E-mail: achim.stahl@rwth-aachen.de

Reactor neutrino experiments played an important role in neutrino physics from the discovery of neutrinos by Cowan and Reines to the current measurements of the mixing angle θ_{13}. I summarize the recent results and give an outlook to the next generation.

XXVII International Symposium on Lepton Photon Interactions at High Energies
17-22 August 2015
Ljubljana, Slovenia

*Speaker.

PoS(LeptonPhoton2015)014

1. Introduction

Nuclear power reactors emit a large flux of electron antineutrinos $\overline{\nu}_e$. Cowan and Reines used this strong source when they first detected neutrinos [1]. Today reactor neutrinos are used to study neutrino oscillations. Neutrinos can either be described by flavor eigenstates or by mass eigenstates. The flavor eigenstates characterize the weak interactions of the neutrinos, while the mass eigenstates are used to propagate the neutrinos in time. The relation between the two descriptions is given by the Pontecorvo-Maki-Nakagawa-Sakata matrix U [2, 3, 6, 7].

$$|\nu_\alpha\rangle = \sum_{i=1}^{3} |U_{\alpha,i}\nu_i\rangle$$

Here $|\nu_\alpha\rangle$ is a state in the flavor basis and $|\nu_i\rangle$ a state in the basis of the mass eigenstates. In the standard parametrization the PMNS-matrix is given by

$$\begin{pmatrix} 1 & 0 & 0 \\ 0 & \cos\theta_{23} & \sin\theta_{23} \\ 0 & -\sin\theta_{23} & \cos\theta_{23} \end{pmatrix} \cdot \begin{pmatrix} \cos\theta_{13} & 0 & \sin\theta_{13}e^{-i\delta} \\ 0 & 1 & 0 \\ -\sin\theta_{13}e^{i\delta} & 0 & \cos\theta_{13} \end{pmatrix} \cdot \begin{pmatrix} \cos\theta_{12} & \sin\theta_{12} & 0 \\ -\sin\theta_{12} & \cos\theta_{12} & 0 \\ 0 & 0 & 1 \end{pmatrix}$$

The first matrix describes the atmospheric oscillation with a $\Delta m^2_{23} \approx 2.4\,10^{-3} eV^2$ and a mixing angle of $\theta_{23} \approx 45°$ at least close to its maximal value. The last matrix describes the solar oscillations with a $\Delta m^2_{12} \approx 7.6\,10^{-5} eV^2$ and a mixing angle of $\theta_{12} \approx 35°$. The central matrix is the topic of this talk. The corresponding Δm^2 is that of the atmospheric oscillations. The mixing angle has recently been measured to be around 9° [4, 5]. The CP-violating phase δ is not known, yet. The measured values of Δm^2_{ij} can be converted into a mass spectrum. It is shown in figure 1. Since neutrino oscillations depend on the mass differences between the states, the baseline of the mass spectrum cannot be determined from neutrino oscillations.

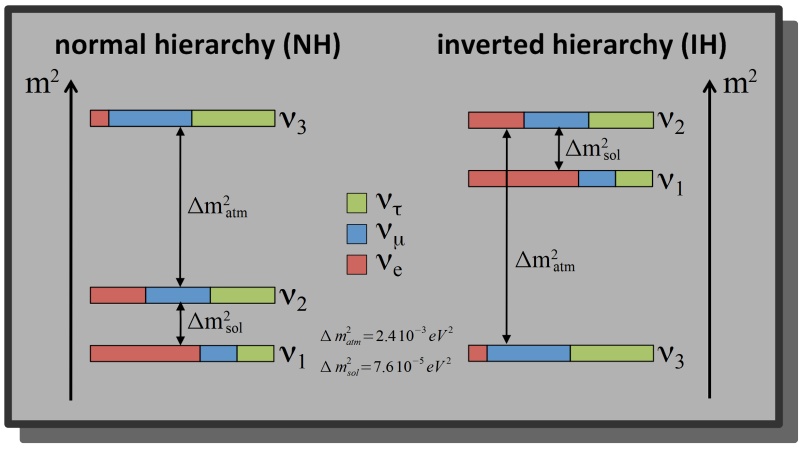

Figure 1: The mass spectrum of the neutrinos in normal and inverted hierarchy.

There are a number of fundamental questions associated with neutrino oscillations. The most important are

- What is the absolute mass scale?
- Is the normal or the inverted mass hierarchy correct?
- Are neutrinos Majorana or Dirac particles?
- Is the CP-symmetry violated in the oscillations?
- Does the PMNS matrix fulfill unitarity?

Reactor neutrino experiments may answer the second question and may contribute to the last question with precision measurements of some of the parameters.

Figure 2 gives an overview of the oscillation patterns expected from reactor neutrinos. Nuclear reactors are a pure source of electron-antineutrinos. The energy is in the range of hundreds of keV to a few MeV. At these energies muon- and tau-antineutrinos are below the kinematic threshold of charged current reactions and cannot be detected. The $\overline{\nu}_e$-disappearance is the only possible measurement. Its probability is shown in the figure together with the range of L/E values covered by the experiment.

2. Reactor Neutrinos

The energy spectrum of neutrinos emitted from the cores of the nuclear power stations is calculated from the β-decays of the neutrino-rich fission fragment. The spectrum of electrons from β-decay can be described as

$$S(E) = K \times F \times pE \times C \times (1+\delta)$$

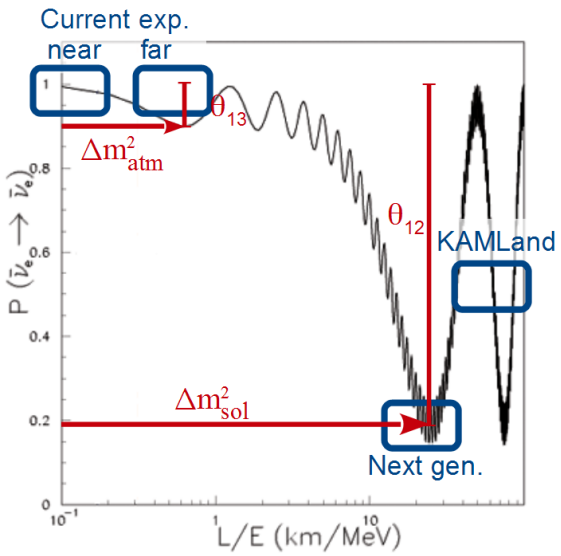

Figure 2: The probability of electron anti-neutrino disappearance.

with the normalization K, the Fermi function F, the phase space factor pE, the shape factor C, and radiative corrections δ. The spectrum of neutrinos is derived from the electron spectrum through its endpoint E_0. For each decay we have

$$E\left(e^-\right) + E\left(\overline{\nu}_e\right) = E_0$$

This is called one branch. The integral neutrino spectrum is derived from these branches through simple summation. The following three summations are applied.

- For each isotope we must sum all possible decay branches taking into account their branching ratios. For example, ^{144}Pr decays directly to the ground-state of ^{144}Nd, but also to excited states at 696 keV and 2.185 MeV. We have to sum the spectra of the three transissions with their proper weights.
- For each fragment of a fission we must sum all the isotopes in its decay chain. For example, if we look at the fission fragment ^{94}Sr, we have to take into account its β-decays, but also those of its instable daughters, in this example ^{94}Y which decays to the practically stable isotope ^{94}Zr.
- For each fuel element we must sum all the fission fragments taking into account their abundance from the fission.

Finally there is one more summation to be done. We have to sum all the fuel elements of the reactor. The relevant ones are ^{235}U, ^{239}Pu, and ^{240}Pu. For a precise calculation we need to take also ^{238}U into account. Only fast neutrons can fission the nucleus which is a rare process, but ^{238}U is the most abundant isotope in the fuel rods and therefore this small probability is visible. This last summation is more challenging, as the composition of the fuel rods changes with time due to the burn-up. The summation must be based on a realistic simulation of each of the reactor cores. This is called the ab initio calculation. Unfortunately for 5 to 10% of decay branches we are missing the data. These branches cannot be calculated ab initio.

A different approach uses experimental data on the electron spectra from the decay. Probes of the isotopes ^{235}U, ^{239}Pu, and ^{240}Pu were activated in the neutron flux of a reactor. The electron spectra were precisely measured for each of the probes [8]. A sum of typically 30 electron spectra $S(E)$ are fitted to the data in an iterative process with the endpoints and the normalizations as free parameters. This procedure does not reproduce the true branches of the decays. The true spectra has hundreds of branches, too many to be fitted. This is simply a theory-inspired parametrization of the electron spectrum. The neutrino spectrum is then derived from the endpoint relation of each branch.

The second method was used for many years until enough nuclear data was available to use at least a combination of both methodes [9]. All branches with sufficiently precise data are calculated ab initio and subtracted from the measured spectra. Only the remaining branches are then parametrized with the second method. The result is shown in figure 3. The new calculation shifted the expected rate up by about 3% increasing the already existing deficit to more than two standard deviations. This is called the reactor anomaly. There is an intensive discussion ongoing about the proper approach to the neutrino spectra and the corrections to be applied. For more details see [10].

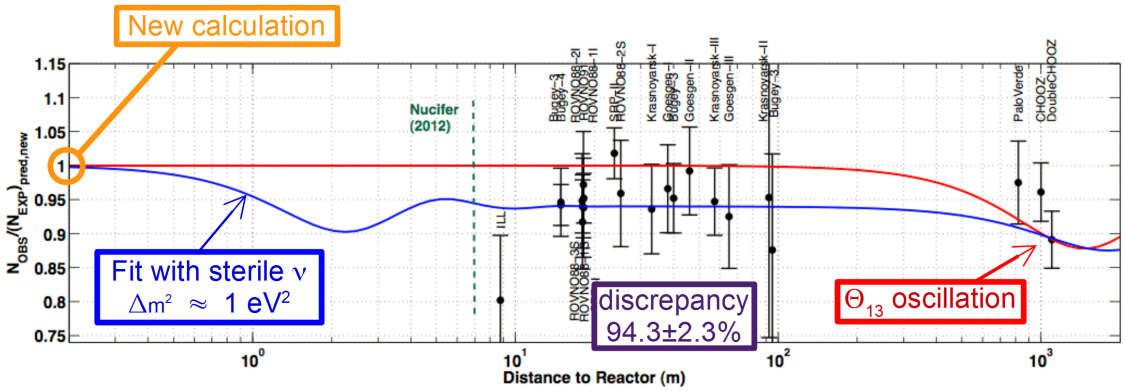

Figure 3: The expected rate of neutrinos as a function of the distance from the reactor cores.

3. Neutrino Detectors

Reactor neutrinos are detected through the inverse β-decay (IBD): $\overline{\nu}_e + p^+ \rightarrow n + e^+$. About 1.8 MeV of the neutrino energy is used up by the creation of the positron and the conversion of the proton into a neutron. This results in a detection threshold. The remaining kinetic energy of the neutrino is transferred to the positron. The recoil of the neutron is almost negligible. The positron looses the energy through excitation of the scintillator and eventually annihilates with an electron in the scintillator. The emitted gammas are captured and add to the light emission of the scintillator. The process is so fast that it cannot be separated in time. It produces the prompt event from which the energy of the neutrino is reconstructed. The neutron is thermalized in the scintillator and finally captured by a nucleus. For example normal hydrogen might capture a neutron, resulting in an excited state of deuterium which emits photons in the transition to the ground state. The thermalization takes a visible amount of time. Therefore the capture of the neutron appears as a delayed event in close spatial correlation with the prompt event. For the capture on hydrogen the typical time-of-delay is 200 μsec and the energy release is 2.2 MeV. In many of the detectors

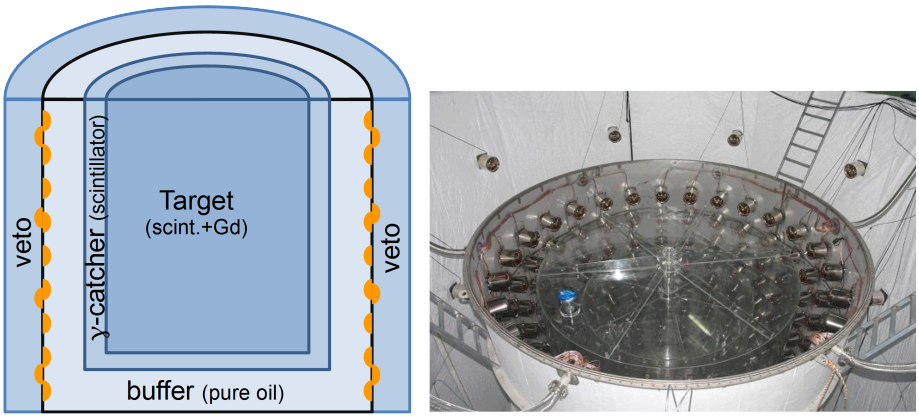

Figure 4: A typical reactor neutrino detector. Left: sketch; right: RENO far detector during construction

gadolinium has been added to the scintillator to speed up the capture process and to increase the energy release. With Gadolinium a typical capture time is 30 μsec and the energy release is 8 MeV.

Figure 4 shows a typical neutrino detector. It is build in cylindrical shells. Neutrinos are detected in the target. The γ-catcher ensures that all photons from the inverse β-decay are captured. The passive buffer (no scintillation) shields the inner volumes from radioactivity from the outside and from the PMTs. These three volumes are separated from each other through transparent acrylic tanks. Together they are mounted in a steel tank that carries the PMTs. Outside of the steel tank is another active volume. It detects muons entering the detector from the outside. On top of the tanks is a muon tracker used to study the background induced by the muons.

4. The Mixing Angle θ_{13}

The most important measurement from reactor neutrinos from the past years is the determination of the third mixing angle θ_{13}. The reactor neutrino experiments give the most precise measurement. The deficit observed at a distance of about 1 km from the cores is driven by this parameter. The impact of other unknown parameters (the mass hierarchy and the CP-violating phase) is negligible. This is different from the situation at the long-baseline experiments. Their observation of ν_e-appearance from a ν_μ-beam (or $\overline{\nu}_e$-appearance from a $\overline{\nu}_\mu$-beam) is strongly affected by θ_{13}, but it also depends on the phase and the hierarchy. In fact there is a complementarity in the results. If we measure θ_{13} from the reactor experiments, the data from the long-baseline experiments gives us information on the hierarchy and the phase.

There are three reactor neutrino experiments to consider. These are Daya Bay in China, Double Chooz in Europe, and Reno in South Korea. Figure 5 compares the three setups. The figures on top show the configurations of near and far detectors with the baselines, the target mass of the detectors, and the thermal power of the cores. Each blue dot represents a core, each red dot a neutrino detector. For example, Daya Bay has four far detectors with a mass of 20 t each. The boxes below give the most important characteristics of the far detectors: the energy resolution for a neutrino energy of 1 MeV, the overburden in meters of water-equivalent, and the statistics collected in summer 2015.

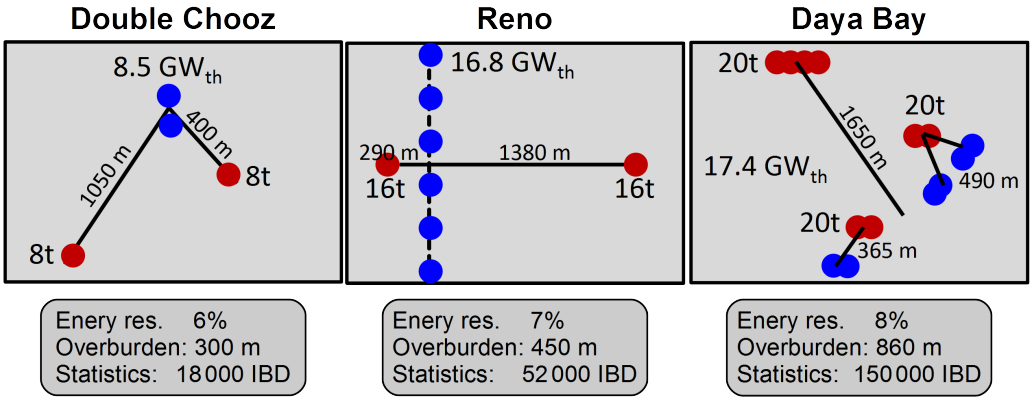

Figure 5: Comparison of the three reactor neutrino experiments.

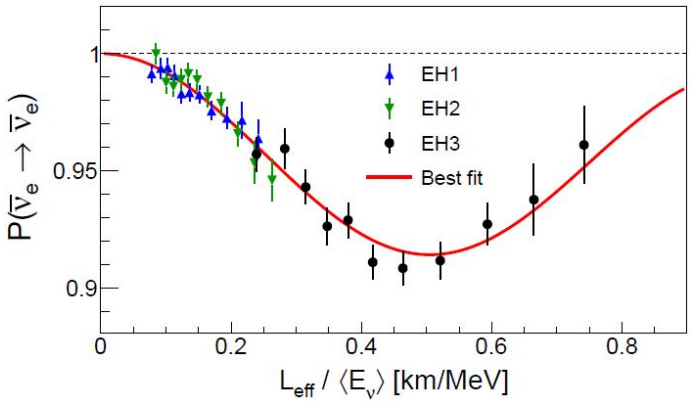

Figure 6: Oscillation pattern from Daya Bay from the ration of far to near detectors [11].

As an example I show the most recent measurement from Daya Bay in figure 6. It is currently the most precise single measurement. It uses IBD events with the neutron captured on Gadolinium. The value of θ_{13} is extracted from a fit to the ratio of neutrinos detected at the far and the near detector. The result is $sin^2 2\theta_{13} = 0.084 \pm 0.005$ [11].

The background in the neutrino samples of the far detectors is critical. It will ultimately be the limiting factor in the precision of the result. The signal consists of a coincidence of a prompt and a delayed event in spatial correlation. The background can be divided into accidental and correlated coincidences. The accidental coincidences are produced by radioactivity in and around the target volume, by fast neutrons produced by cosmic rays in the surrounding rock and entering the detector,

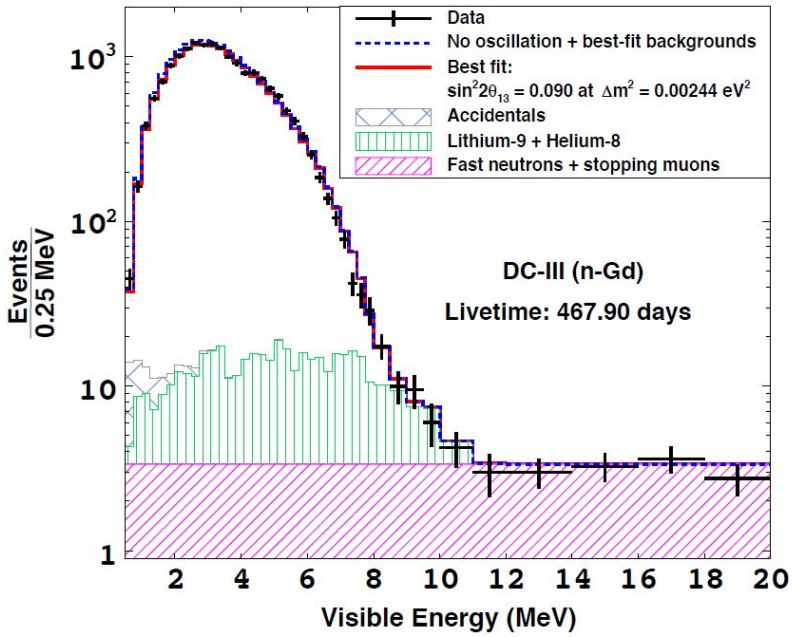

Figure 7: Double Chooz: the IBD spectrum of the far detector with background components [12].

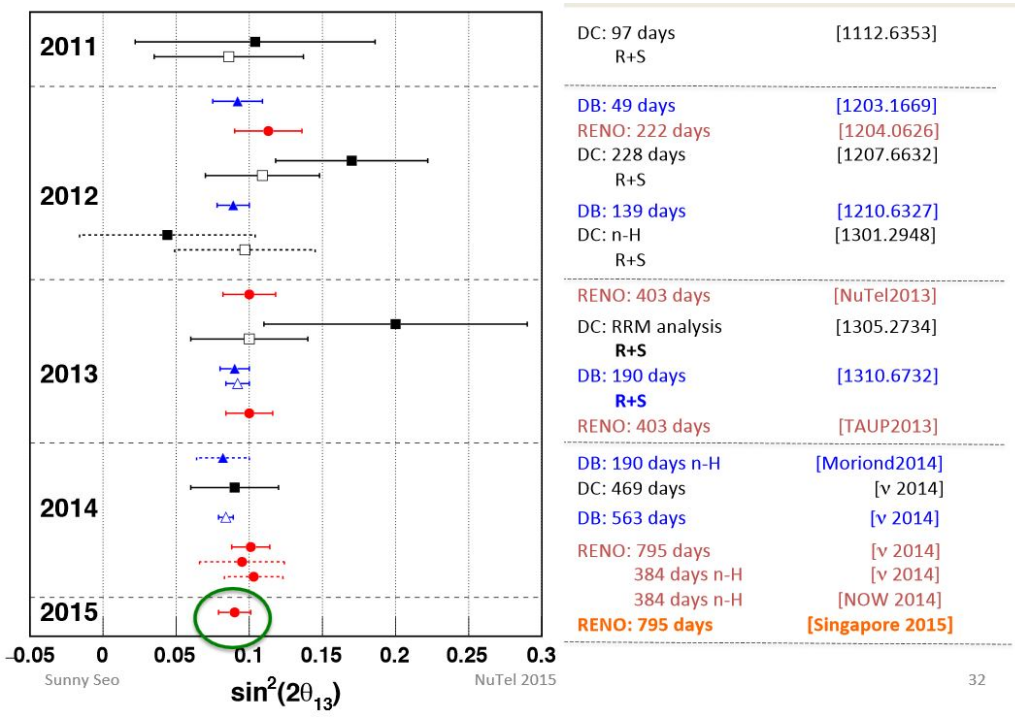

Figure 8: Compilation of results on $sin^2 2\theta_{13}$ [14].

and by muons stopping in the detector. Their rate and energy spectrum can be estimated directly from the data, for example through out-of-time coincidences. This background can be subtracted without severe impact on the precision of the result. It is the correlated background that limits the precision. There are two main components.

- Fast neutrons (MeV-energies) entering the detector and scattering of a proton. If the scatter is hard enough the proton recoil might mimic a prompt signal. Then the neutron thermalizes and creates a delayed signal.

- Cosmogenic background, where a muon enters the detector and destroys a carbon nucleus through spallation. Such an event is relatively easy to detect and will be vetoed. But in a small fraction of reactions isotopes are created in the spallation that create background. These are mainly ^9Li and ^8He. These are meta-stable isotopes. The electron from their β-decay (for example $^9Li \rightarrow ^9 Be + e^- + \overline{\nu}_e$) creates the prompt signal. The daughter nucleus emits a neutron (for example $^9Be \rightarrow ^8 Be + n$) which creates the delayed signal. The background is suppressed by vetos after the impact of a muon in the detector, but the lifetime of the meta-stable isotopes is too long to veto all background.

Both of these backgrounds extend to energies beyond the IBD signal. The background is normalized at high energies and than extrapolated underneath the signal. There are substantial uncertainties in the models of the spectrum which create substantial systematic uncertainties. Figure 7 shows the spectrum of IBD events from Double Chooz [12] with the background from fast neutrons in

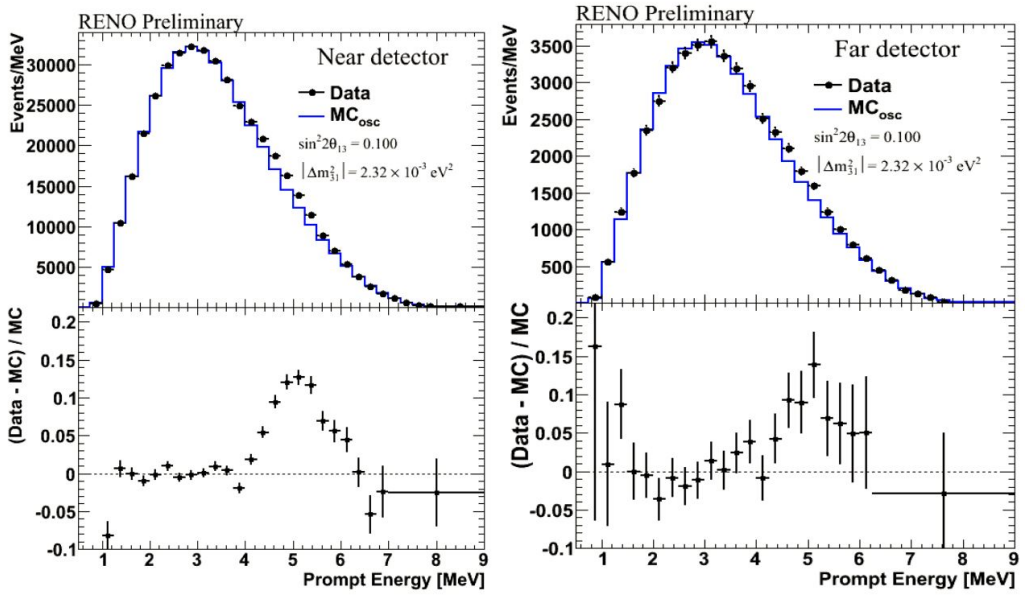

Figure 9: Reno: 5 MeV excess in near (left) and far (right) detector [15].

red and the cosmogenic background in green. A flat spectrum is assumed for the neutrons. The spectrum of the cosmogenic background is derived from nuclear models, from measurements of signals directly after a muon hit the detector, and from data from down-times of the reactor cores for maintenance. Double Chooz has recently presented a new method to estimate the cosmogenic background as a constant rate under a signal that scales proportional to the reactor power in data sets where one or two of the reactor cores where shut down. The result confirms the previous background estimates [13].

Figure 8 summarizes the results. It is taken from a talk of Sunny Seo at Neutrino telescope 2015 [14]. The main result comes from the ratio of antineutrinos detected at the far and the near detector. It is independent of the calculation of the flux or the spectrum from the reactors. However calculations are used for the Monte Carlo simulations and have some impact on the results. Over the years a discrepancy between the calculation and the measurements became evident. An excess of events in the data of about 1% to 1.5% at energies around 5 MeV developed. Figure 9 shows the excess in the data of the near and far detectors of RENO. All three experiments see a similar excess. Reno showed that the excess scales with the reactor power of the data sets. Therefore it cannot be an external background. It is unexplained. It must be either a systematic effect common to all three experiments or a deficit in the calculation of the reactor spectrum.

5. The Mass Hierarchy

The next generation of reactor neutrino experiments will address the question of the mass hierarchy [16]. They are located in the first oscillation maximum of the solar oscillation which is about 50 to 60 kilometers from the reactors (see figure 2). The oscillation pattern is depicted in figure 10. The probability for the disappearance of electron antineutrinos is given by ($\Delta m^2_{ij} =$

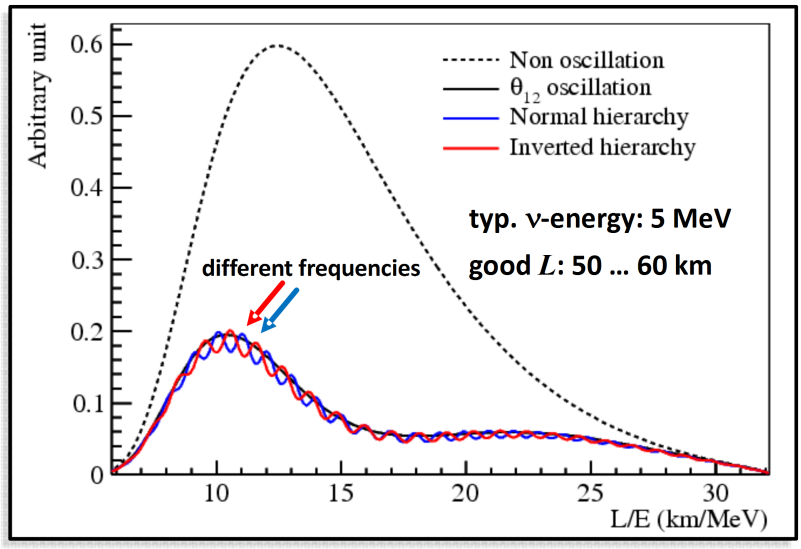

Figure 10: Oscillation pattern at the first solar oscillation maximum for normal and inverted mass hierarchy.

$m_i^2 - m_j^2$)

$$P_{\overline{\nu}_e \to \overline{\nu}_e} = 1 - sin^2 2\theta_{13}\, sin^2 \frac{\Delta m^2_{ee} L}{4E} - cos^4 \theta_{13}\, sin^2 2\theta_{12}\, sin^2 \frac{\Delta m^2_{21} L}{4E}$$

with

$$sin^2 \frac{\Delta m^2_{ee} L}{4E} = cos^2 \theta_{12}\, sin^2 \frac{\Delta m^2_{31} L}{4E} + sin^2 \theta_{12}\, sin^2 \frac{\Delta m^2_{32} L}{4E}$$

The first term describes the solar oscillation. The second term has a frequency Δm^2_{ee} which is a superposition of the two frequencies m^2_{32} and m^2_{31}. The first one is known from atmospheric neutrinos. The second one is slightly larger or smaller depending on the hierarchy (see figure 1). The neutrino spectrum exhibits a beating between these two frequencies which changes with the mass hierarchy. The mass hierarchy is determined from the measurement of this frequency. The JUNO experiment will attempt to do this measurement besides a number of other interesting astrophysical topics. It was approved in 2014. Construction started with the beginning of this year. Data taking is supposed to start in 2020 (see [17]). RENO50 is another proposal in this direction.

References

[1] F. Reines et al., *Detection of the Free Antineutrino*, *Phys. Rev.* **117** (1960) 159.

[2] B. Pontecorvo, *Inverse beta processes and nonconservation of lepton charge*, *JETP* **7** (1958) 172.

[3] Z. Maki et al., *Remarks on the Unified Model of Elementary Particles*, *Prog. of Theo. Phys.* **28** (1962) 870.

[4] K. Abe et al., *First Muon-Neutrino Disappearance Study with an Off-Axis Beam*, *Phys. Rev. Lett.* **107** (2011) 041801.

[5] Y. Abe et al., *Indication for the disappearance of reactor electron antineutrinos in the Double Chooz experiment*, *Phys. Rev. Lett.* **108** (2012) 131801.

[6] F. P. An et al., *Observation of electron-antineutrino disappearance at Daya Bay*, *Phys. Rev. Lett.* **108** (2012) 171803.

[7] J. K. Ahn et al., *Observation of Reactor Electron Antineutrino Disappearance in the RENO Experiment*, *Phys. Rev. Lett.* **108** (2012) 191802

[8] K. Schreckenbach et al., *Determination of the Antineutrino Spectrum from ^{235}U Thermal Neutron Fission Products up to 9.5 MeV*, *Phys. Lett. B* **160** (1985) 325.

[9] T. A. Mueller et al., *Improved Predictions of Reactor Antineutrino Spectra*, *Phys. Rev. C* **83** (2011) 054615.

[10] G. Mention et al., *The Reactor Antineutrino Anomaly*, *Phys. Rev. D* **83** (2011) 073006.

[11] F. P. An et al., *New Measurement of Antineutrino Oscillation with the Full Detector Configuration at Daya Bay*, *Phys. Rev. Lett.* **115** (2015) 11, 111802.

[12] Y. Abe et al., *Improved measurements of the neutrino mixing angle θ_{13} with the Double Chooz detector*, *JHEP* **1410** (2014) 086.

[13] P. Novella, *Double Chooz: First Background-independent Measurement of θ_{13}*, *Phys. Procedia* **61** (2015) 502.

[14] S. H. Heo, *New results from RENO*, talk presented at *Neutrino Telescopes 2015*, Venice, March 2015.

[15] S. H. Seo et al., *New Results from RENO and The 5 MeV Excess*, *AIP Conf. Proc.* **1666** (2015) 080002, [arXiv:1410.7987 hep-ex].

[16] Y. F. Li et al., *Unambiguous Determination of the Neutrino Mass Hierarchy Using Reactor Neutrinos*, *Phys. Rev. D* **88** (2013) 013008.

[17] F. An et al., *Neutrino Physics with JUNO*, [arXiv:1507.05613].